Models of iron speciation and concentration in the stratified epipelagic ocean

Song-Miao Fan[1] and John P. Dunne[1]

Received 23 May 2011; revised 6 July 2011; accepted 8 July 2011; published 12 August 2011.

[1] Surface ocean iron speciation is simulated using a time-dependent box-model of light-mediated redox cycling over a range of aeolian inputs of soluble iron in the stratified epipelagic ocean. At steady-state, Dissolved iron (DFe) concentration increases with aeolian input of soluble iron up to 0.1 μmol m^{-2} d^{-1}, and is limited by the solubility of ferric hydroxide at higher fluxes which causes the formation of colloidal iron. We demonstrate that even in the presence of ample excess ligand, rapid conversion of dissolved iron between oxidized and reduced forms in the tropical surface ocean exposes DFe to colloid formation and scavenging. This result provides an explanation for the much smaller range of interregional variability in DFe measurements (0.05–0.4 nM) than soluble Fe fluxes (0.01–1 μmol m^{-2} d^{-1}) and dust fluxes (0.1–10 g m^{-2} yr^{-1}) predicted by atmospheric models. We incorporate the critical behavior of the full chemical speciation model into a reduced, computationally efficient model suitable for large scale calculations.
Citation: Fan, S.-M., and J. P. Dunne (2011), Models of iron speciation and concentration in the stratified epipelagic ocean, *Geophys. Res. Lett.*, *38*, L15611, doi:10.1029/2011GL048219.

1. Introduction

[2] Dissolved iron concentration is a key variable that controls phytoplankton processes in the surface ocean [*Morel and Price*, 2003]. Uptake of iron by phytoplankton has been shown to occur with the dissolved inorganic iron species [*Hudson and Morel*, 1990; *Sunda and Huntsman*, 1995; *Fujii et al.*, 2011]. Direct phytoplankton uptake of iron bound to organic ligands is slow compared to the uptake of inorganic iron [*Maldonado et al.*, 2005; *Shaked et al.*, 2005]. Low concentrations of dissolved iron in seawater limit phytoplankton iron uptake and growth in the Equatorial Pacific, subarctic Pacific, and the Southern Ocean, where large-scale artificial iron fertilization have resulted in phytoplankton blooms [*Boyd et al.*, 2007].

[3] In regions of low dust deposition (e.g., Equatorial Pacific, tropical South Pacific, parts of the Southern Ocean), measured dissolved iron concentrations range from 0.05 nM to 0.1 nM in the surface layer; while in regions of high dust deposition, such as the tropical Atlantic, surface water measurements range from 0.2 to 0.4 nM (Table S1 (within Text S1) in the auxiliary material).[1] This range (0.05–0.4 nM) is remarkably smaller than the three orders of magnitude range in atmospheric iron deposition fluxes [*Fan et al.*, 2006]. Aeolian input, biological uptake, remineralization and sedimentation of biogenic particles, scavenging by and dissolution of lithogenic particles, upwelling and vertical mixing, and light-mediated redox chemistry can all influence the concentration of iron in the epipelagic ocean [*Jickells*, 1999; *Wu et al.*, 2001; *Croot et al.*, 2004; *Bergquist et al.*, 2007]. Modelers have struggled to represent this complex behavior in global biogeochemical models in a mechanistically robust yet computationally efficient manner, and have chosen algorithms necessarily empirical in scope in order to represent iron limitation. First attempts included *Archer and Johnson* [2000] and *Fung et al.* [2000] who attempted simple scavenging representations, *Moore et al.* [2004] invoked a single empirical threshold scavenging response, while *Parekh et al.* [2004] explored various ligand and scavenging representations. In this study, a box model including 24 equations relevant to iron redox cycling, coagulation, uptake, and scavenging is used to evaluate factors controlling dissolved iron in the stratified epipelagic ocean. The model is described in Section 2; results and discussions are presented in Section 3; a summary of main conclusions is given in Section 4.

2. Model Description

[4] The complexity of iron chemistry has made operational definition difficult. Dissolved iron (DFe) includes inorganic ferrous ions, denoted by Fe(II)′, and inorganic ferric species, Fe(III)′, and organic complexes, FeL measured in seawater after 0.02 μm or 0.2 μm filtration [*Nishioka et al.*, 2001; *Wu et al.*, 2001]. While a filter pore size of 0.4 μm is sometimes considered operationally 'dissolved', this phase may include significant colloidal iron, CFe, mainly amorphous hydroxide. Conversely, iron bound to large (>0.2 μm) polysaccharides is portioned into FeL in this study. Particulate iron (PFe, >0.4 μm) may be biogenic or lithogenic or aggregate of aged forms of ferric oxyhydroxide that dissociate more slowly than fresh colloids.

[5] During the day, light-mediated redox cycling maintains iron speciation in a dynamic state with colloidal and complexed iron photodissociation to dissolved inorganic iron (Fe′ = Fe(II)′ + Fe(III)′) [*Croot et al.*, 2005]. At night, iron speciation is near thermodynamic equilibrium with FeL dominating the dissolved species [*Weber et al.*, 2005]. Iron is also contained in live cells of phytoplankton, bacteria, and virus, with a lifetime of 1–10 days [*Strzepek et al.*, 2005]. Grazing and lysis release iron into the dissolved and particulate pools.

[6] Many of the elemental processes that influence the dynamic state of iron speciation in seawater have been

[1]Geophysical Fluid Dynamics Laboratory, NOAA, Princeton, New Jersey, USA.

[1]Auxiliary materials are available in the HTML. doi:10.1029/2011GL048219.

Table 1. Aqueous-Phase Reaction Rate Constants

Reaction Number	Reaction	K $M^{(1-n)}s^{-1}$	n	References/Notes
R01	$Fe(II)' + O_2 \rightarrow Fe(III)' + O_2^-$	10.	2	*Millero et al.* [1987]
R02	$Fe(II)' + H_2O_2 \rightarrow Fe(III)' + OH + OH^-$	7.2×10^4	2	*Millero and Sotolongo* [1989]
R03	$Fe(II)' + O_2^- \rightarrow Fe(III)' + H_2O_2$	1.0×10^7	2	*Rush and Bielski* [1985]
R04	$Fe(III)' + O_2^- \rightarrow Fe(II)' + O_2$	1.5×10^8	2	*Rush and Bielski* [1985]
R05	$Fe(III)' + Ligand \rightarrow FeL$	2.0×10^6	2	*Witter et al.* [2000]
R06	$FeL \rightarrow Fe(III)' + Ligand$	1.0×10^{-6}	1	*Witter et al.* [2000]
R07	$Fe(III)' + CFe \rightarrow CFe$	2.0×10^6	2	*Rose and Waite* [2003]
R08	$CFe \rightarrow CFe + Fe(III)'$	2.0×10^{-5}	1	*Rose and Waite* [2003]
R09	CFe + Particle (mg/L) → PFe	1.5×10^{-5}	2	*Dunne et al.* [1997]
R10	$Fe' + Cells \rightarrow$ Export production	4.0×10^{-7}	1	See text
R11	$Fe(III)' + h\nu \rightarrow Fe(II)' + OH$	1.5×10^{-5}	1	See footnote[a]
R12	$FeL + h\nu \rightarrow Fe(II)' + Ligand$	1.0×10^{-3}	1	See footnote[a]
R13	$CFe + h\nu \rightarrow Fe(II)'$	1.5×10^{-5}	1	See footnote[a]
R14	$PFe + h\nu \rightarrow Fe(II)'$	2.3×10^{-8}	1	See footnote[a]
R15	PFe → sinking loss	6.4×10^{-7}	1	See text
R16	$FeL + O_2^- \rightarrow Fe(II)' + O_2$	1.5×10^5	2	*Rose and Waite* [2005]
R17	FeL + H.B. → Fe(II)′	3.0×10^{-6}	1	Heterotrophic Bacteria
R18	$CDOM + h\nu \rightarrow O_2^-$	8.0×10^{-7}	1	See footnote[a]
R19	$HO_2 + O_2^- (+ H^+) \rightarrow H_2O_2 + O_2$	1.0×10^8	2	*Bielski* [1978]
R20	H_2O_2 (+ ROM) → products	5.8×10^{-6}	1	*Moore et al.* [1993]
R21	$Cu(I)' + O_2 \rightarrow Cu(II)' + O_2^-$	4.6×10^5	2	*Bjergbakke et al.* [1976]
R22	$Cu(I)' + H_2O_2 \rightarrow Cu(II)' + OH + OH^-$	7.0×10^3	2	*Berdnikov* [1973]
R23	$Cu(I)' + O_2^- (+ 2H^+) \rightarrow Cu(II)' + H_2O_2$	9.4×10^9	2	*von Piechowski et al.* [1993]
R24	$Cu(II)' + O_2^- \rightarrow Cu(I)' + O_2$	8.0×10^9	2	*Rabani et al.* [1973]

[a]All photoreaction (R11-R14, R18) rate coefficients are given for a diurnal average, clear sky solar irradiance at 32°N on equinox.

measured and are listed with representative values for rate constants at 25°C in Table 1. A detailed description of the box model for iron redox cycling in the surface ocean over a diel cycle is given by *Fan* [2008]. Briefly, the model calculates the rates of production and loss processes in the surface mixed layer according to the law of mass action. Given an initial state of species concentrations, the time rate of change for each species is integrated forward in time, with the concentrations updated every time step, until a stationary state is reached. The model assumes all species are well mixed in a 30 m surface layer. Iron cycling through biological uptake is balanced by remineralization and a net removal of iron by sedimentation of biogenic particulate iron for conditions of high remineralization and low export consistent with observational estimates [*Landry et al.*, 1997]. Other forms of particulate iron are removed from the surface ocean by sedimentation. The diurnal cycle of solar radiation in the model is set for 32°N at Spring Equinox and for clear sky. The concentration of CDOM is specified to be 3 μM, organic matter reacting with H_2O_2 to be 10 nM, particulate matter to be 0.05 mg/L, and total ligand to be 1.8 nM iron equivalent. The concentrations of reactive oxygen species and iron species are calculated online with the model using the reactions in Table 1.

[7] Iron redox cycling and speciation in the stratified epipelagic ocean is simulated for dust deposition fluxes typical of the tropical North Atlantic and northern Indian (10 g m^{-2} yr^{-1}), North Pacific, extratropical Atlantic, and Southwest Pacific (1 g m^{-2} yr^{-1}) and tropical Pacific, subtropical South Pacific, and much of the Southern Ocean (0.1 g m^{-2} yr^{-1}) based on sediment trap measurements and global dust transport modeling [*Tegen et al.*, 2002]. Soluble Fe fluxes are calculated from the dust fluxes and model simulated aerosol Fe solubility [*Fan et al.*, 2006]. The conditions specified in the simulations do not apply in regions with significant iron supply from below such as high-latitudes, coasts [*Johnson et al.*, 1999], and upwelling zones [*Slemons et al.*, 2010]. In the intensely iron limited regions such as the Southern Ocean, we would need to incorporate the seasonality of mixed layer light limitation, major nutrient and iron supply from below and ecosystem dynamics - all factors and iron speciation chemistry that we plan to consider simultaneously in a global ocean general circulation model.

3. Results and Discussions

[8] Simulations with a constant dust deposition rate of 10 g m^{-2} yr^{-1} and readily soluble iron fractions 1% to 5% result in nearly constant dissolved iron at 0.3 nM while the sum of dissolved and colloidal iron increases from 0.5 nM at 1% solubility to 0.9 nM at 5% solubility (Figure 1). This compares well to measurements in the surface ocean from 25°S to 30°N in the Atlantic, 0.2–0.4 nM for DFe and 0.2–0.9 nM for CFe + DFe [*Bergquist et al.*, 2007]. Measurements of aerosol iron solubility in this region range from 0.5% at high dust to 30% at very low dust concentrations [*Chen and Siefert*, 2004; *Buck et al.*, 2010].

[9] At a lower dust deposition rate of 1 g m^{-2} yr^{-1} and 2% solubility, modeled DFe is 0.17 nM with no colloidal iron (Figure 1). At 4% solubility DFe is 0.21 nM and CFe begins to form (0.02 nM). At even higher assumptions of solubility from 6% to 10%, DFe is constant at 0.22 nM while CFe increases from 0.03 nM to 0.06 nM. Measurements of DFe (<0.2 μm) in regions have a large total range from 0.05 to 0.4 nM but primarily between 0.1–0.2 nM, while those of CFe + DFe (<0.4 μm) are generally higher with a range from 0.2–0.7 nM (Table S1). Total and soluble aerosol iron deposition fluxes in these regions may be much higher than the annual average during dust active season, causing dissolved iron elevated above saturation with respect to ferric hydroxide and substantial formation of colloidal iron.

[10] At the low dust deposition flux of 0.1 g m^{-2} yr^{-1}, DFe increases linearly with aerosol iron solubility, from 0.04–

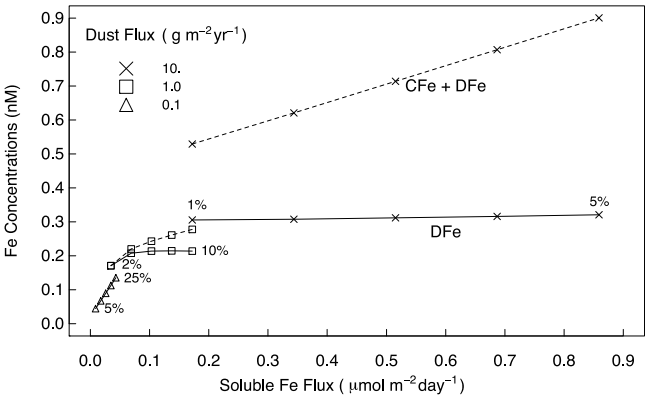

Figure 1. Steady-state concentrations (solid line for [DFe] and dashed line for [DFe] + [CFe], averaged over 24 hours) vs. soluble Fe flux. Results are shown for a constant dust deposition of: 10 g m^{-2} yr^{-1} and soluble Fe fractions ranging from 1–5 percent, 1 g m^{-2} yr^{-1} and soluble Fe fractions ranging from 2–10 percent, 0.1 g m^{-2} yr^{-1} and soluble Fe fractions ranging from 5–25 percent. Light-induced dissolution of particulate iron provides an additional source of 0.36, 0.034, and 0.003 μmol m^{-2} d^{-1}, respectively for the three dust fluxes.

0.14 nM for the simulated solubility range of 5–25 percent, while CFe is zero (Figure 1). This result is in good agreement with measurements of DFe in the Equatorial Pacific south of the upwelling zone and tropical-subtropical South Pacific (Table S1). Given the large observed variability in dust fluxes, model results suggest that DFe could be 2–3 times higher in more dusty years in low flux regions.

[11] The solubility of ferric hydroxide, determined by the ratio of rate coefficients R08/R07 (Table 1), emerges as a key factor controlling dissolved iron in stratified surface oceans. At soluble Fe fluxes >0.1 μmol m^{-2} d^{-1}, colloidal iron is formed when Fe(III)′ concentration is greater than the equilibrium solubility of ferric hydroxide (0.01 nM at 25°C [*Liu and Millero*, 2002]). This and the partitioning of DFe (=Fe(II)′ + Fe(III)′ + FeL) set by the redox cycling together maintain a relatively constant DFe even as the soluble Fe flux increases. As a result, the range of DFe in the epipelagic ocean is small compared to the range of dust deposition fluxes. At lower soluble Fe fluxes (<0.1 μmol m^{-2} d^{-1}) colloidal Fe is not formed. DFe are very low and variable as a response to dust deposition and aerosol iron solubility in large areas of the global ocean receiving low dust deposition perpetually or for extended periods of time.

[12] At high soluble iron fluxes, colloidal iron forms and is scavenged, strongly buffering the dissolved iron concentration as soluble iron flux increases (Figure 1). Exposure to light in the presence of ligands serves to both make Fe(III) more bio-available through reduction and disassociation and also to make Fe(III) more susceptible to colloidal formation and scavenging, leading to the apparent fixed upper limit on dissolved Fe concentrations in high dust deposition regions. This result provides a mechanistic interpretation of dissolved and colloidal iron measurements in the tropical Atlantic [*Bergquist et al.*, 2007] and a tidy justification for the relatively ad hoc but apparently robust approach used by *Moore et al.* [2004].

[13] There remain significant uncertainties in rate coefficients (Table 1) used in the model. For an analysis of sensitivity, a series of simulations were carried out with one model parameter altered in each case (Figures S1–S9 in the auxiliary material). The biggest effect is the enhancement of FeL under conditions of complete darkness (Figure S4) in which simple ligand chemistry takes control. The dependency of dissolved Fe to soluble iron supply is also sensitive to mixed layer depth (Figure S2). The maximum dissolved Fe level was found to be sensitive to the rate constants for formation (Figure S6) and photodissociation (Figure S3) of FeL. Both the soluble supply and the maximum dissolved Fe level were found to be sensitive to the dissociation of colloidal Fe (Figure S5), formation of FeL (Figure S6) and the reaction between Fe(III) and superoxide (Figure S8). While these sensitivities determine the absolute structure of the Fe response to iron supply, they do not change the overall character and suggest that some tuning of the more uncertain of these constants (e.g., the photodissociation of FeL and dissociation of colloidal Fe) may be sufficient for robust global ocean applications.

[14] Having explored the competitive influence of ligand exchange, photochemistry and colloid exchange, we now apply this understanding towards construction of a reduced model amenable to large scale ocean biogeochemical applications [e.g., *Parekh et al.*, 2004]. In order to represent the complex dynamical behavior described in this work in a computationally efficient manner, we have distilled the full model down to a simplified representation based on a three tracer system of dissolved (DFe), colloidal (CFe) and particulate (PFe) iron based on the kinetic equations shown in Table 1. Their chemical tendencies are calculated as follows:

$$\begin{aligned}
dPFe/dt &= K_{10}\cdot Fe(III) - (K_{15}+K_{14})\cdot PFe + K_{09}\cdot P\cdot CFe \\
&\quad + K_{10}\cdot Fe(II) \\
dCFe/dt &= \left(K_{07}\cdot\left(CFe + C_{Bkg}\right)\cdot Fe(III) - (K_{13}+K_{08}+K_{09}\cdot P)\right. \\
&\quad \left.\cdot CFe\right) \\
dDFe/dt &= -\left(K_{10}+K_{07}\cdot\left(CFe+C_{Bkg}\right)\right)\cdot Fe(III) + K_{14}\cdot PFe \\
&\quad + K_{08}\cdot CFe + K_{13}\cdot CFe - K_{10}\cdot Fe(II) + R_{dep}
\end{aligned}$$

While the speciation of DFe is assumed to be at instantaneous steady state due to rapid redox cycling:

$$\begin{aligned}
dFe(III)/dt &= -\left(K_{10}+K_{09}+K_{04}\cdot O_2^- + K_{07}\cdot\left(CFe+C_{Bkg}\right)\right) \\
&\quad \cdot Fe(III) + K_{25}\cdot PFe + K_{06}\cdot FeL + K_{08}\cdot CFe \\
&\quad + \left(K_{01}\cdot O_2 + K_{02}\cdot H_2O_2 + K_{03}\cdot O_2^-\right)\cdot Fe(II) \\
&\quad - K_{05}\cdot L_{Free}\cdot Fe(III) + R_{dep} = 0 \\
dFeL/dt &= K_{05}\cdot L_{Free}\cdot Fe(III) - (K_{06}+K_{sum}\cdot)FeL = 0 \\
dFe(II)/dt &= \left(K_{09}+K_{04}\cdot O_2^-\right)\cdot Fe(III) + K_{14}\cdot PFe + K_{sum}\cdot FeL \\
&\quad + K_{13}\cdot CFe - \left(K_{10}+K_{01}\cdot O_2 + K_{02}\cdot H_2O_2\right. \\
&\quad \left. + K_{03}\cdot O_2^-\right)\cdot Fe(II) = 0 \\
dL_{Free}/dt &= \left((K_{06}+K_{sum})\cdot FeL - K_{05}\cdot L_{Free}\cdot Fe(III)\right) = 0
\end{aligned}$$

where $K_{sum} = K_{12} + K_{16}O_2^- + K_{17}$. The (quadratic) equations may be solved for the iron species and free ligand, given concentrations of total ligand (L_{Total}), O_2, H_2O_2 and O_2^- in

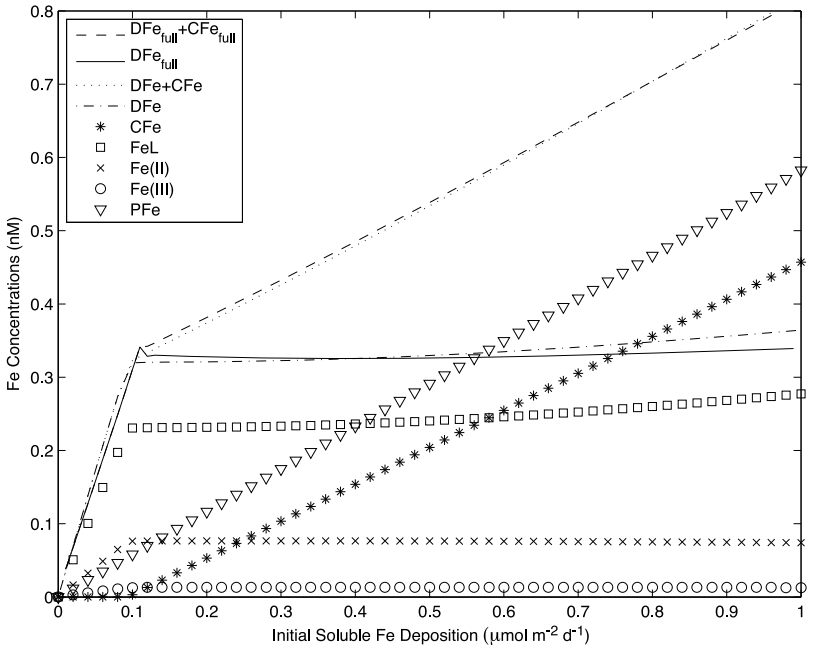

Figure 2. Steady-state concentrations (averaged over 24 hours) vs. soluble Fe flux in the reduced version of the model described in the text compared to the full model both including only initially soluble iron deposition.

the seawater and the photochemical reaction rate coefficients for specified irradiance and temperature:

$$a = K_{05} \cdot \left(1 + \left(K_{09} + K_{04} \cdot O_2^- K_{sum}\right) / \left(K_{01} \cdot O_2 + K_{02} \cdot H_2O_2 + K_{03} \cdot O_2^- + K_{10} + K_{sum}\right)\right)$$

$$b = K_{05} \cdot (L_{Total} - DFe) + K_{06} + K_{sum} + (K_{06} + K_{sum}) \cdot \left(K_{09} + K_{04} \cdot O_2^- - K_{sum}\right) / \left(K_{01} \cdot O_2 + K_{02} \cdot H_2O_2 + K_{03} \cdot O_2^- + K_{10} + K_{sum}\right) + K_{05} \cdot \left(K_{sum} \cdot DFe + K_{14} \cdot PFe + K_{08} \cdot CFe\right) / \left(K_{01} \cdot O_2 + K_{02} \cdot H_2O_2 + K_{03} \cdot O_2^- + K_{10} + K_{sum}\right)$$

$$c = \left(K_{06} + K_{sum}\right) \cdot \left(\left(K_{sum} \cdot DFe + K_{14} \cdot PFe + K_{08} \cdot CFe\right) / \left(K_{01} \cdot O_2 + K_{02} \cdot H_2O_2 + K_{03} \cdot O_2^- + K_{10} + K_{sum}\right) - DFe\right)$$

$$Fe(III) = \left(-b + \left(b^2 - 4 \cdot a \cdot c\right)^{1/2}\right) \Big/ (2 \cdot a)$$

$$FeL = Fe(III) / ((K_{06} + K_{sum}) / K_{05} + Fe(III)) \cdot L_{Total}$$

$$Fe(II) = DFe - Fe(III) - FeL$$

$$L_{Free} = L_{Total} - FeL$$

For specified L_{total} and O_2 (3×10^{-4}M) and concentrations of H_2O_2 (1×10^{-7}M) and O_2^- (1×10^{-9}M during the day) predicted by the full model, iron speciation calculated using the reduced model is compared with the full model in Figure 2 across the continuum of initial soluble iron deposition fluxes (ignoring in-situ dust iron dissolution after deposition for ease of comparison). By avoiding the need to explicitly track all tracers and to represent processes that occur on the timescales of seconds to a few hours, we arrive at a representation of iron cycling that retains the overall mechanistic behavior of the full model yet tractable for interpretation and amenable for implementation in biogeochemical/ecological models. When implemented in an ocean biogeochemistry model, this reduced algorithm will allow ocean circulation to operate on dissolved Fe species as a group while accounting for a strong day-to-night variation of iron speciation with important consequences for iron uptake and scavenging. Our next step will be to imbed this representation of iron chemistry in a full global biogeochemical model.

4. Summary

[15] This study investigates the controls of dissolved iron concentration using a model of light-mediated redox cycling of iron and reactive oxygen species in the epipelagic ocean. The model results suggest that iron redox, ligand and scavenging cycling combine to maintain dissolved iron in the stratified surface ocean within a fairly narrow range in the face of large variability in supply through atmospheric deposition of soluble iron. Dissolved iron increases with aeolian input of soluble iron in regions of low dust deposition, either perpetually or for extended periods of time. Dissolved iron is buffered to a constant level (narrow range) in regions of high dust deposition by formation of colloidal iron when concentration of inorganic iron, Fe(III)′, is greater than the equilibrium solubility of ferric hydroxide. These conclusions are in agreement with observations of dissolved iron in the world ocean. A reduced model of iron speciation is also derived to represent the critical behavior of the full chemical model in a computationally efficient manner suitable for large scale calculations.

[16] **Acknowledgments.** Charles Stock and Robbie Toggweiler provided useful comments. Hiram Levy II encouraged this research. We thank two anonymous reviewers for their useful comments.

[17] The Editor thanks two anonymous reviewers for their assistance in evaluating this paper.

References

Archer, D. E., and K. Johnson (2000), A model of the iron cycle in the ocean, *Global Biogeochem. Cycles*, *14*, 269–279, doi:10.1029/1999GB900053.

Berdnikov, V. M. (1973), Catalytic activity of the hydrated copper ion in the decomposition of hydrogen peroxide, *Russ. J. Phys. Chem.*, *47*, 1060–1062.

Bergquist, B. A., J. Wu, and E. A. Boyle (2007), Variability in oceanic dissolved iron is dominated by the colloidal fraction, *Geochim. Cosmochim. Acta*, *71*, 2960–2974, doi:10.1016/j.gca.2007.03.013.

Bielski, B. H. J. (1978), Reevaluation of the spectral and kinetic properties of HO_2 and O_2^- free radicals, *Photochem. Photobiol.*, *28*, 645–649, doi:10.1111/j.1751-1097.1978.tb06986.x.

Bjergbakke, E., K. Sehested, and O. L. Rasmussen (1976), The reaction mechanism and rate constants in the radiolysis of Fe^{2+}/Cu^{2+} solutions, *Radiat. Res.*, *66*, 433–442, doi:10.2307/3574449.

Boyd, P. W., et al. (2007), Mesoscale iron enrichment experiments 1993–2005: Synthesis and future directions, *Science*, *315*, 612–617, doi:10.1126/science.1131669.

Buck, C. S., W. M. Landing, and J. A. Resing (2010), Particle size and aerosol iron solubility: A high-resolution analysis of Atlantic aerosols, *Mar. Chem.*, *120*, 14–24, doi:10.1016/j.marchem.2008.11.002.

Chen, Y., and R. L. Siefert (2004), Seasonal and spatial distribution and dry deposition fluxes of atmospheric total and labile iron over the tropical and subtropical North Atlantic Ocean, *J. Geophys. Res.*, *109*, D09305, doi:10.1029/2003JD003958.

Croot, P. W., P. Streu, and A. R. Baker (2004), Short residence time for iron in surface seawater impacted by atmospheric dry deposition from Saharan dust events, *Geophys. Res. Lett.*, *31*, L23S08, doi:10.1029/2004GL020153.

Croot, P. L., et al. (2005), Spatial and temporal distribution of Fe(II) and H_2O_2 during EisenEx, and open ocean mescoscale iron enrichment, *Mar. Chem.*, *95*, 65–88, doi:10.1016/j.marchem.2004.06.041.

Dunne, J. P., J. W. Murray, J. Young, L. Balistrieri, and J. K. B. Bishop (1997), ^{234}Th and particle cycling in the central equatorial Pacific, *Deep Sea Res., Part II*, *44*, 2049–2083, doi:10.1016/S0967-0645(97)00063-5.

Fan, S.-M. (2008), Photochemical and biochemical controls on reactive oxygen and iron speciation in the pelagic surface ocean, *Mar. Chem.*, *109*, 152–164, doi:10.1016/j.marchem.2008.01.005.

Fan, S.-M., W. J. Moxim, and H. Levy II (2006), Aeolian input of bioavailable iron to the ocean, *Geophys. Res. Lett.*, *33*, L07602, doi:10.1029/2005GL024852.

Fujii, M., T. C. Dang, A. L. Rose, T. Omura, and T. D. Waite (2011), Effect of light on iron uptake by the freshwater cyanobacterium *Microcystis aeruginoa*, *Environ. Sci. Technol.*, *45*, 1391–1398, doi:10.1021/es103311h.

Fung, I., S. Meyn, I. Tegen, S. C. Doney, J. John, and J. K. B. Bishop (2000), Iron supply and demand in the upper ocean, *Global Biogeochem. Cycles*, *14*, 281–296, doi:10.1029/1999GB900059.

Hudson, R. J. M., and F. M. M. Morel (1990), Iron transport in marine phytoplankton: Kinetics of cellular and medium coordination reactions, *Limnol. Oceanogr.*, *35*, 1002–1020, doi:10.4319/lo.1990.35.5.1002.

Jickells, T. D. (1999), The inputs of dust derived elements to the Sargasso Sea: A synthesis, *Mar. Chem.*, *68*, 5–14, doi:10.1016/S0304-4203(99)00061-4.

Johnson, K. S., F. P. Chavez, and G. E. Friederich (1999), Continental-shelf sediment as a primary source of iron for coastal phytoplankton, *Nature*, *398*, 697–700, doi:10.1038/19511.

Landry, M. R., et al. (1997), Iron and grazing constraints on primary production in the central equatorial Pacific: An EqPac Synthesis, *Limnol. Oceanogr.*, *42*, 405–418, doi:10.4319/lo.1997.42.3.0405.

Liu, X., and F. J. Millero (2002), The solubility of iron in seawater, *Mar. Chem.*, *77*, 43–54, doi:10.1016/S0304-4203(01)00074-3.

Maldonado, M., R. F. Strzepek, S. Sander, and P. W. Boyd (2005), Acquisition of iron bound to strong organic complexes, with different Fe binding groups and photochemical reactivities, by phytoplankton communities in Fe-limited subantarctic waters, *Global Biogeochem. Cycles*, *19*, GB4S23, doi:10.1029/2005GB002481.

Millero, F., and S. Sotolongo (1989), The oxidation of Fe(II) with H_2O_2 in seawater, *Geochim. Cosmochim. Acta*, *53*, 1867–1873, doi:10.1016/0016-7037(89)90307-4.

Millero, F., S. Sotolongo, and M. Izaguirre (1987), The oxidation kinetics of Fe(II) in seawater, *Geochim. Cosmochim. Acta*, *51*, 793–801, doi:10.1016/0016-7037(87)90093-7.

Moore, C. A., C. T. Farmer, and R. G. Zika (1993), Influence of the Orinoco River on hydrogen peroxide distribution and production in the eastern Caribbean, *J. Geophys. Res.*, *98*(C2), 2289–2298, doi:10.1029/92JC02767.

Moore, J. K., S. C. Doney, and K. Lindsay (2004), Upper ocean ecosystem dynamics and iron cycling in a global 3D model, *Global Biogeochem. Cycles*, *18*, GB4028, doi:10.1029/2004GB002220.

Morel, F. M. M., and N. M. Price (2003), The biogeochemical cycles of trace metals in the oceans, *Science*, *300*, 944–947, doi:10.1126/science.1083545.

Nishioka, J., S. Takeda, C. S. Wong, and K. W. Johnson (2001), Size-fractionated iron concentrations in the northeast Pacific Ocean: Distribution of soluble and small colloidal iron, *Mar. Chem.*, *74*, 157–179, doi:10.1016/S0304-4203(01)00013-5.

Parekh, P., M. J. Follows, and E. Boyle (2004), Modeling the global ocean iron cycle, *Global Biogeochem. Cycles*, *18*, GB1002, doi:10.1029/2003GB002061.

Rabani, J., D. Klug-Roth, and J. Lilie (1973), Pulse radiolytic investigations of the catalyst diproportionation of peroxy radicals. Aqueous cupric ions, *J. Phys. Chem.*, *77*, 1169–1175, doi:10.1021/j100628a018.

Rose, A. L., and T. D. Waite (2003), Predicting iron speciation in coastal waters from kinetics of sunlight-mediated iron redox cycling, *Aquat. Sci.*, *65*, 375–383, doi:10.1007/s00027-003-0676-3.

Rose, A. L., and T. D. Waite (2005), Reduction of organically complexed ferric iron in seawater, *Environ. Sci. Technol.*, *39*, 2645–2650, doi:10.1021/es048765k.

Rush, J. D., and B. H. J. Bielski (1985), Pulse radiolytic studies of the reactions of HO_2/O_2^- with Fe(II)/Fe(III) ions. The reactivity of HO_2/O_2^- with ferric ions and its implication on the occurrence of the Haber-Weiss reaction, *J. Phys. Chem.*, *89*, 5062–5066, doi:10.1021/j100269a035.

Shaked, Y., A. D. Kustka, and F. M. M. Morel (2005), A general kinetic model for iron acquisition by eukaryotic phytoplankton, *Limnol. Oceanogr.*, *50*(3), 872–882, doi:10.4319/lo.2005.50.3.0872.

Slemons, L. O., J. W. Murray, J. Resing, B. Paul, and P. Dutrieux (2010), Western Pacific coastal sources of iron, manganese, and aluminum to the Equatorial Undercurrent, *Global Biogeochem. Cycles*, *24*, GB3024, doi:10.1029/2009GB003693.

Strzepek, R. F., M. T. Maldonado, J. L. Higgins, J. Hall, K. Safi, S. W. Wilhelm, and P. W. Boyd (2005), Spinning the "ferrous wheel": The importance of the microbial community in an iron budget during the FeCycle experiment, *Global Biogeochem. Cycles*, *19*, GB4S26, doi:10.1029/2005GB002490.

Sunda, W., and S. Huntsman (1995), Iron uptake and growth limitation in oceanic and coastal phytoplankton, *Mar. Chem.*, *50*, 189–206, doi:10.1016/0304-4203(95)00035-P.

Tegen, I., S. P. Harrison, K. Kohfeld, I. C. Prentice, M. Coe, and M. Heimann (2002), Impact of vegetation and preferential source areas on global dust aerosol: Results from a model study, *J. Geophys. Res.*, *107*(D21), 4576, doi:10.1029/2001JD000963.

von Piechowski, M., T. Nauser, T. Hoigne, and R. E. Buhler (1993), O_2^- decay catalysed by Cu^{2+} and Cu^+ ions in aqueous solutions: A pulse radiolysis study of atmospheric chemistry, *Ber. Bunsenges. Phys. Chem*, *97*, 762–771.

Weber, L., C. Volker, M. Schartau, and D. A. Wolf-Gladrow (2005), Modeling the speciation and biogeochemistry of iron at the Bermuda Atlantic Time-series Study site, *Global Biogeochem. Cycles*, *19*, GB1019, doi:10.1029/2004GB002340.

Witter, A., D. Hutchins, A. Butler, and G. Luther III (2000), Determination of conditional stability constants and kinetic constants for strong model Fe-binding ligands in seawater, *Mar. Chem.*, *69*, 1–17, doi:10.1016/S0304-4203(99)00087-0.

Wu, J., E. Boyle, W. Sunda, and L. Wen (2001), Soluble and colloidal iron in the oligotrophic North Atlantic and North Pacific, *Science*, *293*, 847–849, doi:10.1126/science.1059251.

J. P. Dunne and S.-M. Fan, Geophysical Fluid Dynamics Laboratory, NOAA, 201 Forrestal Rd., Princeton, NJ 08542, USA. (songmiao.fan@noaa.gov)